# Performance characterization on downwash flow and spray drift of multirotor unmanned agricultural aircraft system based on CFD

Hongze Li[1], Hang Zhu[1*], Zihao Jiang[1], Yubin Lan[2,3*]

(1. *School of Mechanical and Aerospace Engineering, Jilin University, Changchun 130022, China*;
2. *School of Agricultural Engineering and Food Science, Shandong University of Technology, Zibo 255000, Shandong, China*;
3. *Department of Biological and Agricultural Engineering, Texas A&M University, Texas, 77843, USA*)

**Abstract:** In recent years, multi-rotor Unmanned Aerial Vehicles (UAVs) have been employed in the field of plant protection in China. Spray drift has been considered a major impact in agriculture aerial spraying, and spray quality in the application of plant protection products. The downwash including wake vortices and downward wind field plays a major role in the dispersal and deposition of pesticide spray released by nozzle(s) equipped in aircraft. Differ from the fixed-wing UAV, the downwash flow of multi-rotor UAV resulted from the rotation of the rotor. Therefore, a study on off-target drift and ground deposit concerning the rotor rotation was simulated through a series of Computational Fluid Dynamics (CFD) simulations to obtain the influence of downwash. The discrete Phase Model (DPM) was taken to simulate the motion of droplet particles since it is an appropriate way to simulate discrete phases in the flow field and can track particle trajectory. In this study, the parameters of CFD simulations were acquired by three kinds of actual replicated experiments. The simulation analysis mainly obtains the droplet drift and deposition rule, the influence of eddy current, and downwash flow caused by the rotor rotation. The results showed that the downwash distribution below different rotors was different owing to the flight angle of inclination, "behind" is the greatest, "middle" is secondly, and "forward" is the smallest in value(behind, middle, and forward represent three regions below rotors along flight direction). According to the simulation results, two methods of reducing droplet drift were put forward and specific simulations were carried out to prove their feasibility. The results of this study can provide theoretical support for improving the spray quality of UAVs and reducing the drift of droplets.

**Keywords:** Unmanned Aerial Vehicles, spray drift, downward wind field, rotor rotation, eddy current, downwash distribution
**DOI:** 10.25165/j.ijabe.20221503.7315

**Citation:** Li H Z, Zhu H, Jiang Z H, Lan Y B. Performance characterization on downwash flow and spray drift of multirotor unmanned agricultural aircraft system based on CFD. Int J Agric & Biol Eng, 2022; 15(3): 1–8.

## 1 Introduction

The traditional agricultural application usually performs the task by manual operations or semi-mechanized methods in China[1,2]. Unmanned Aerial Vehicle (UAV) aerial pesticide application has clear advantages compared with traditional inspection methods. First, UAV application is less costly in labor and more effective than traditional methods under the premise of enhancing the spray effect. A significant labor advantage is of great significance when using UAV applications. Second, remote control avoids pesticide harm to the skin. However, more research is needed in this area because the use of UAVs under the influence of natural airflow enhances the possibility of droplet drift[3,4].

In the 1970s, the United States Department of Agriculture (USDA) Forest Service and the U.S. Army supported the continued development and application of mathematical spray dispersion models because these models helped to determine the interactions of many factors that affect spray operations. Two currently available computer models are the Agricultural Diffusion (AGDISP) model[5] and the Forest Service Cramer-Barry-Grim (FSCBG) model. The AGDISP near wake model solves the Lagrangian system of equations for the location and position variation of the spray material released from each nozzle on the aircraft. The FSCBG model predicts the transport and behavior of pesticide sprays released from aircraft, influenced by aircraft wake and local atmospheric conditions[6]. Based on the AGDISP model, the AgDRIFT model[7-10] was developed jointly by the Spray Drift Research Group, EPA, and the Forest Service in the USA. The aforementioned studies have mainly focused on manned fixed-wing aircraft and helicopters, but relatively few analyses have been conducted on small Unmanned Aerial Vehicles.

Multirotor Plant Protection Unmanned Aerial Vehicle, a common type of Unmanned Aerial Vehicle, is made for aerial application of pesticides or fertilizer. The important role of pesticides or plant protection products in modern agriculture in reducing pest infestations and increasing yields is undeniable[11,12]. Aerial spraying works involving pesticides released into the atmosphere above the crop or forest at a certain height, with the purpose of dispersing the pesticide product amongst the plant foliage, or soil. Xue et al.[13] designed a UAV-based automatic control spraying system to perform plant-protection operations. The test of route precision and multiple-spraying swath uniformity demonstrated the high spray uniformity of the UAV with this system. Wingtip vortices produced by roll-up downstream of the aircraft wing are a natural consequence of multirotor UAV lift generation and aircraft flight. Pesticide application influenced by downwash is normally undertaken using field experiments that are conducted under prevailing meteorological conditions. Jiao et

**Received date:** 2022-01-02 **Accepted date:** 2022-05-18
**Biographies: Hongze Li**, PhD candidate, research interest: intelligent machinery of precision agriculture and automatic control, Email: lihz18@mails.jlu.edu.cn; **Zihao Jiang**, Master candidate, research interest: precise pesticide spraying, Email: labmem000@foxmail.com.
***Corresponding author: Hang Zhu**, PhD, Associate Professor, research interest: precision agriculture aviation and equipment. School of Mechanical and Aerospace Engineering, Jilin University NO.5988, Renmin Road, Changchun 130022, China. Tel: +86-18088665997, Email: hangzhu@jlu.edu.cn; **Yubin Lan**, PhD, Professor, research interest: precision agriculture aviation and equipment. College of Electronic Engineering, South China Agricultural University, Guangzhou 510642, China. Tel: +86-13922707507, Email: ylan@scau.edu.cn.

al.[14] proposed a new method that uses infrared thermal imaging technology to detect the thermal difference before and after spraying, and then measures the range and concentration distribution of droplets to monitor pesticide drift in aerial sprays. Li et al.[15] acquired the spatial distribution of spraying droplets and vertical wind speed through wind speed sensors and sample nodes in the canopy, 30 cm beneath the canopy and 60 cm beneath the canopy. Guo et al.[16] studied the droplets deposition effects including deposition amount, coverage rate, and droplet size in different vortex states by collecting droplets collected by water sensitive paper (WSP). However, it is often difficult, time-consuming, and expensive to conduct numerous field experiments because of the variability and complexity involved. Compared to undertaking a set of experiments in the field, running a virtual simulation experiment through mathematical models by computer is fast and reproducible to estimate the likely spray drift movement onto plants or soil surfaces. As a general rule, such mathematical models should include as much physics and chemistry as is necessary to describe the important processes involved, but should not be overly complicated or contain too many input parameters[17,18]. Wen et al.[19] used the computational fluid dynamics method to simulate the downwash flow field of a quad-rotor drone based on the lattice Boltzmann method (LBM). Ryan et al.[20] used a Lagrangian approach to model spray dispersal in the near wake of the aircraft, this method becomes computationally infeasible to model far downstream locations due to the large number of Lagrangian droplets needed to achieve statistical convergence. Zhang et al.[21] investigated the velocity field of the wake of a Thrush 510G carrying out spray application close to the ground. The results showed that the aircraft normally operates in extreme ground effect and wake vortices play a major role in the dispersal and deposition of pesticide spray released behind the aircraft. Yang et al.[22] proposed an approach to research the influence of the downwash and windward airflow on the motion distribution of droplet group for the SLK-5 six-rotor plant protection UAV. Omar et al.[23] studied the airflow of aerial crop spraying systems including the effect of aircraft speed and nozzle orientation on the distribution of spray droplets at a certain height using CFD. Fesal et al.[11] simulated off-target drift and ground deposit onto a 250 m strip through a series of Computational Fluid Dynamic (CFD) simulations. There have been many analyses of downwash in hover state, but relatively fewer analyses concerned with the influence of rotation speed difference and flight angle of inclination in actual operation.

Previous studies derived a droplet drift model influenced by three factors: wind speed $X_w$ (m/s), pressure $X_p$ (MPa), and spray height $X_h$ (m). Droplet drift and deposition patterns were simulated and analyzed under different operating conditions, and droplet drift and deposition phenomena were explored but did not focus on the effect of downwash[24]. In the actual experiment, two common phenomena that should be noticed were found. First, UAV fly process includes rotation speed difference of different rotors and flight angle of inclination. Second, rotation speed difference and flight angle of inclination vary at different fly speeds. Therefore, this study aimed to simulate and analyze the flow field in the droplet motion domain and the droplet drift motion affected by downwash concerning the above two factors.

## 2 Field experiment

### 2.1 Experiment design

MG-1P eight-rotor plant protection UAV (DJI, Shenzhen, China), a common type applied in the realm of plant protection, and detailed parameters are listed in Table 1. A field experiment was carried out to acquire flight angle of inclination and rotor speed at different operation speeds. The data acquired can provide support for subsequent simulation analysis.

Along with the variety of operation speeds, the rotor rotation speed is always changing, leading to various downwash. In the actual experiment, operation speed was set as 1-3 m/s, 3-5 m/s, and 5-7 m/s corresponding to “slow”, “middle”, and “fast” in the actual operation of plant protection UAV. The test used a standard operating load (10 kg) and each test was repeated three times to ensure accurate results. The experiment data were analyzed by software “DJI Assistant 2” (DJI, Shenzhen, China). The overall experiment series are listed in Table 2.

**Table 1 Parameters of DJI MG-1P eight-rotor plant protection UAV**

| Parameter | Value | Parameter | Value |
|---|---|---|---|
| Dimensions /mm×mm×mm | 1460×1460×578 | Liquid tank volume/L | 10 |
| Diagonal wheelbase/mm | 1500 | Nozzle | XR11001VS |
| Total weight/kg | 9.7 | Nozzle Quantity | 4 |

**Table 2 Overall experiment series**

| Experiment series | Operation speed/m·s$^{-1}$ | Correspond speed |
|---|---|---|
| 1 | 1-3 | Slow |
| 2 | 3-5 | Middle |
| 3 | 5-7 | Fast |

### 2.2 Parameters analysis by actual experiment

According to the data acquired by “DJI Assistant 2”, the speed of the symmetrical rotor is similar, the main rotation speed difference happens to forward and behind rotors, and the rotation direction of every rotor is contrary. The explanation for this is the flight path was almost a straight flight forward. Therefore, the eight rotors were divided into three groups, “forward”, “middle”, and “behind”, as shown in Figure 1. The rotation direction of 2, 4, 6, and 8 was clockwise and 1, 3, 5, and 7 was counterclockwise. The data statistics of three flight strategy groups covered flight angle of inclination and rotor speed are listed in Table 3.

As shown in Table 3, when the operation speed was 1-3 m/s, the flight angle of inclination was 2.46° and the maximum rotation speed difference was 500 r/min. When the operation speed was 3-5 m/s, the flight angle of inclination was 5.19° and the maximum rotation speed difference was 600 r/min. When the operation speed was 5-7 m/s, the flight angle of inclination was 10.28° and the maximum rotation speed difference was 1100 r/min. It is clear that the rotor speed and flight angle of inclination vary under different flight operation speeds. The operation speed is positively correlated with flight angle of inclination and rotation speed. The experimental parameters including rotor rotation speed and flight angle of inclination were the basis of subsequent simulation analysis.

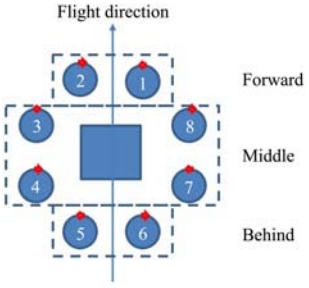


Figure 1 Direction of rotation and divided groups

**Table 3 Data statistics of three flight strategy groups covered flight angles of inclination and rotor speeds**

| Operation speed /m·s$^{-1}$ | Groups | Rotor speed /r·min$^{-1}$ | Flight angle of inclination/(°) |
|---|---|---|---|
| 1-3 | Forward | 4500 | 2.46 |
| | Middle | 4700 | |
| | Behind | 5000 | |
| 3-5 | Forward | 4500 | 5.19 |
| | Middle | 4800 | |
| | Behind | 5100 | |
| 5-7 | Forward | 4600 | 10.28 |
| | Middle | 5000 | |
| | Behind | 5700 | |

## 3 Simulation analysis

### 3.1 Geometric model building

When considering the downwash flow of MG-1P plant protection UAV, the rotor is the most important component. Therefore, the three-dimensional laser scanner Handy Scan 700 (Figure 2a) (Creaform, Quebec, Levis, Canada) was used to scan the rotor, then the 3D modeling of the rotor (Figure 2b) was constructed using the UG8.5 (UGS PLM Software, California, USA) by dealing with the point cloud. A cuboid model (Figure 2c) was established in software ANSYS ICEM CFD 15.0 (NASDAQ: ANSS, Canonsburg, PA, USA). The length, width, and height of the simulation calculation area were set as 10 m, 20 m, and 10 m to simulate the spraying area, the rotor was set as 3 m away from the top surface to avoid the distortion and impact, on the total grid area of 4 700 000 (Figure 2d). Grids of rotors are encrypted to have a better spatial resolution (Figure 2e). The nozzle is positioned directly 20 cm below the rotor and the nozzle distance is 150 cm according to the technical parameters of MG-1P.

a. Laser scanner handy scan

b. Rotor model

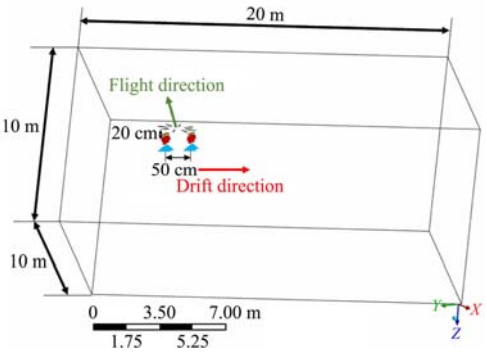


c. Computational domain and boundary setup

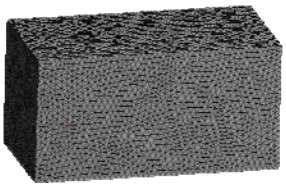

d. Overall grid

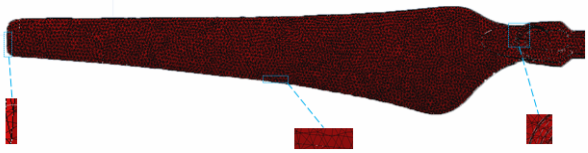

e. Rotor grid encrypted.

Figure 2 Computational domain and boundary setup

The simulation analysis mainly obtains the droplet deposition rule and downwash distribution law caused by the rotor rotation. The boundary conditions are set as follows: The left face of the cuboid is the velocity inlet; the bottom face is the wall pressure outlet; the other four surfaces are all pressure outlets; the outlets are set as boundary escapes. In the simulation analysis, the continuous phase substance is air and the discrete uses the parameters of liquid water to simulate chemicals. In the steady-state calculation mode, the standard $k$-$\varepsilon$ model (ANSYS, 15.0) was selected to simulate the turbulent wind flow. Its transport equations are shown in Equations (1) and (2).

$$\frac{\partial(\rho k)}{\partial t}+\frac{\partial(\rho k u_i)}{\partial x_i}=\frac{\partial}{\partial x_j}[(\mu+\frac{\mu_t}{\sigma_k})\frac{\partial k}{\partial x_j}]+G_k+G_b-\rho\varepsilon-Y_M+S_k \quad (1)$$

$$\frac{\partial(\rho\varepsilon)}{\partial t}+\frac{\partial(\rho\varepsilon u_i)}{\partial x_i}=\frac{\partial}{\partial x_j}[(\mu+\frac{\mu_t}{\sigma_\varepsilon})\frac{\partial\varepsilon}{\partial x_j}]+ C_{1\varepsilon}\frac{\varepsilon}{k}(G_k+C_{3\varepsilon}G_b)-C_{2\varepsilon}\rho\frac{\varepsilon^2}{k}+S_\varepsilon \quad (2)$$

where, $k$ is the turbulence kinetic energy, m$^2$/s$^2$; $\varepsilon$ is the turbulence dissipation rate, %; $t$ is the time constant, s; $x_i$, $x_j$ are components in $x$-axis direction, m; $\mu$ is the dynamic viscosity, kg/m·s; $\mu_t$ is the turbulence viscosity, kg/m·s; $\rho$ is the density of the fluid, kg/m$^3$; $u_i$ is velocity, m/s, $G_k$ is generated by turbulent kinetic energy caused by the average velocity gradient, kg/s$^3$·m; $G_b$ is generated by turbulent kinetic energy caused by buoyancy, kg/s$^3$·m; $Y_M$ is a pulsating expansion term in compressible turbulence; $C_{1\varepsilon}$, $C_{2\varepsilon}$, and $C_{3\varepsilon}$ are empirical constants, Prandtl numbers of $\sigma_k$ and $\sigma_\varepsilon$ correspond to turbulent kinetic energy $k$ and turbulent dissipation rate respectively; $S_k$ and $S_\varepsilon$ are the user-defined source items.

### 3.2 Design of simulation experiment

The control variates method was used to solve the problem including multivariate by changing one of the factors. The definition of flight angle of inclination was taken by rotating computational domain to simulate real flight situation. The computational domain was rotated at three angles (2.46°, 5.19°, and 10.28°), respectively (10.28° in Figure 3). Three rotor rotation speeds were defined by profiles and the overall control variates of the parameters are shown in Table 4.

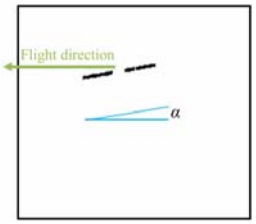


Note: $\alpha$ means the flight angle of inclination (2.46°, 5.19°, 10.28°) corresponding to three operation speeds.

Figure 3 Schematic of Computational domain rotation

**Table 4 Simulation variates setup of test parameters**

| Wind Speed/m·s$^{-1}$ | Operation Speed/m·s$^{-1}$ | | |
|---|---|---|---|
| | 1-3 | 3-5 | 5-7 |
| 0 | $A_1$ | $B_1$ | $C_1$ |
| 1 | $A_2$ | $B_2$ | $C_2$ |
| 3 | $A_3$ | $B_3$ | $C_3$ |

Note: A, B, C represent different three levels of operation speed, 1-3 m/s, 3-5 m/s, 5-7 m/s; 1, 2, 3 represent different wind speeds, 0 m/s, 1 m/s, 3 m/s.

### 3.3 Discrete phase setting

Computational Fluid Dynamics (CFD) has become an increasingly popular tool used to predict model and study turbulent, multiphase flow systems[25,26] and the ability of Discrete Phase Model (DPM) has been shown to accurately simulate particle dispersion and deposition[27,28]. In this study, the flat fan atomizer model of the DPM was selected to simulate the XR11001 nozzle of Teejet Company (Wheaton, IL, USA). In the DPM model, Euler method is used to describe the continuous phase. Navier-Stokes equation[29] is used to obtain velocity and other parameters. The discrete phase is described by Lagrange method, and its movement is obtained by integrating the motion equations of a large number of particles. Therefore, this model is called Euler-Lagrange model[30], and its transport equation can be expressed as

$$\frac{d_{up}}{dt}=\frac{18\mu C_D\,\mathrm{Re}}{24\rho_p dp^2}(u-u_p)+\frac{g_x(\rho_p-\rho)}{\rho_p}+\frac{1}{2}\frac{\rho}{\rho_p}\frac{d}{dt}(u-u_p) \quad (3)$$

where, $u$ is the continuous phase velocity, m/s; $u_p$ is the velocity of particle, kg/m$^3$; $\rho_p$ is the density of particle; $d_p$ is the particle diameter, m; $g_x$ is the acceleration of gravity, 9.8 m/s$^2$ in this case; Re is the relative Reynolds number; $C_D$ is the drag coefficient. The parameter settings of the nozzle are listed in Table 5.

**Table 5 Parameters of the flat fan atomizer used to simulate XR11001 nozzle**

| Parameter | Value |
|---|---|
| X-center/m | 0.75/2.25 |
| Y-center/m | 2 |
| Z-center/m | 1.494 |
| X-virtual center/m | 0.75/2.25 |
| Y-virtual center/m | 2 |
| Z-virtual center/m | 1.5 |
| X-fan normal vector | 0 |
| Y-fan normal vector | −1 |
| Z-fan normal vector | 1 |
| Flow rate/kg·s$^{-1}$ | 0.01316 |
| Spray half angle/(°) | 55 |
| Orifice Width/m | 0.00091 |
| Droplet diameter/$\mu$m | 130-250 |
| Flat fan sheet constant | 3 |
| Atomizer dispersion angle/(°) | 6 |

The time step was 0.01 s, with a maximum limit of 200 iterations for a total of 2 s simulation time. DPM model configuration in the solver is listed in Table 6.

**Table 6 Parameters for DPM setup**

| Parameter | Value |
|---|---|
| Interaction with continuous phase | On |
| Unsteady particle tracking | On |
| Inject particles | Particle time step |
| Particle time step size/s | 0.01 |
| Drag law | Spherical |
| Two-way coupling turbulence | On |

### 3.4 Dynamic mesh and other Parameter Settings

The simulation of rotor rotation was realized by eight profiles for eight rotors in dynamic mesh settings. The rotation direction was divided into clockwise (CW) and counterclockwise (CCW) corresponding to different groups of rotors and rotation speed settings followed by Table 3 acquired by field experiment. Smoothing and remeshing in mesh methods were selected to display mesh motion.

The variation of air density under standard atmospheric pressure and normal temperature is less than 5%, it is regarded as an incompressible fluid, and the pressure-based solver type is selected. All the simulations are based on transient calculations. The convergence criterion is set to $10^{-5}$, which means that the converged solutions are reached when the residuals of several significant variables are equal to or less than $10^{-5}$. The standard discretization scheme was used for the pressure and the second-order upwind scheme for the momentum, turbulent kinetic energy, and turbulent dissipation rate equations.

## 4 Results

### 4.1 Analysis of the downwash wind field

Downwash is the most meaningful for droplet particle deposition and drift reduction. For the purpose of research space distribution of downwash, six contour planes below the rotor were selected, 0.25 m, 0.50 m, 0.75 m, 1.00 m, 1.25 m, and 1.50 m (Figure 4). As shown in Figure 5, their downwash distribution map within 3 m of the domain center in a horizontal direction was expressed.

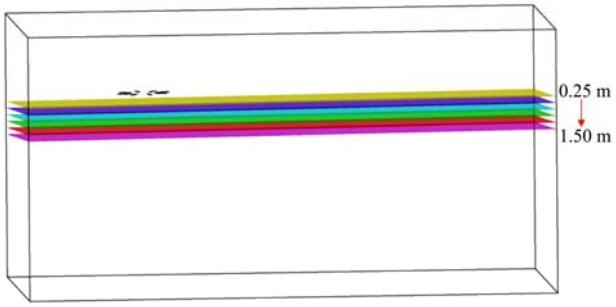


Note: Six contour planes below the rotor were selected in different colors, from the upward to the downward are 0.25 m, 0.50 m, 0.75 m, 1.00 m, 1.25 m, and 1.50 m.

Figure 4 Contour plane below the rotor

Several conclusions can be acquired according to the law of downwash distribution. Downwash around the rotor is the biggest and decreases to the center and all sides. Due to the rotor rotation speed difference, the downwash produced by the behind rotor was larger than the front rotor. Downwash around the nozzles on the left and right sides were the same and the downwash around the nozzles on the front and behind sides were different in value.

The analysis below was the general law of downwash distribution and lacks specific evolution of downwash. Two lines were established in computational domain to obtain the distribution of downwash in horizontal direction (Figure 6a) and vertical direction (Figure 6b). Based on established lines, the law of downwash changes in $X$ and $Z$ directions is shown in Figure 7.

Several conclusions can be acquired according to Figure 7a. Downwash around "behind" rotors is bigger than "forward" and the biggest difference was 1.63 m/s. Downwash around the "center" region is the smallest and the difference with "behind" rotors was 5.17 m/s.

Several other conclusions can be acquired according to

Figure 7b. Downwash below the rotor is 9.36 m/s and the location was 0.32 m below the rotor. The distance between the rotor plane and the nozzles should be smaller than 0.32 m for the purpose of acquiring a larger initial velocity.

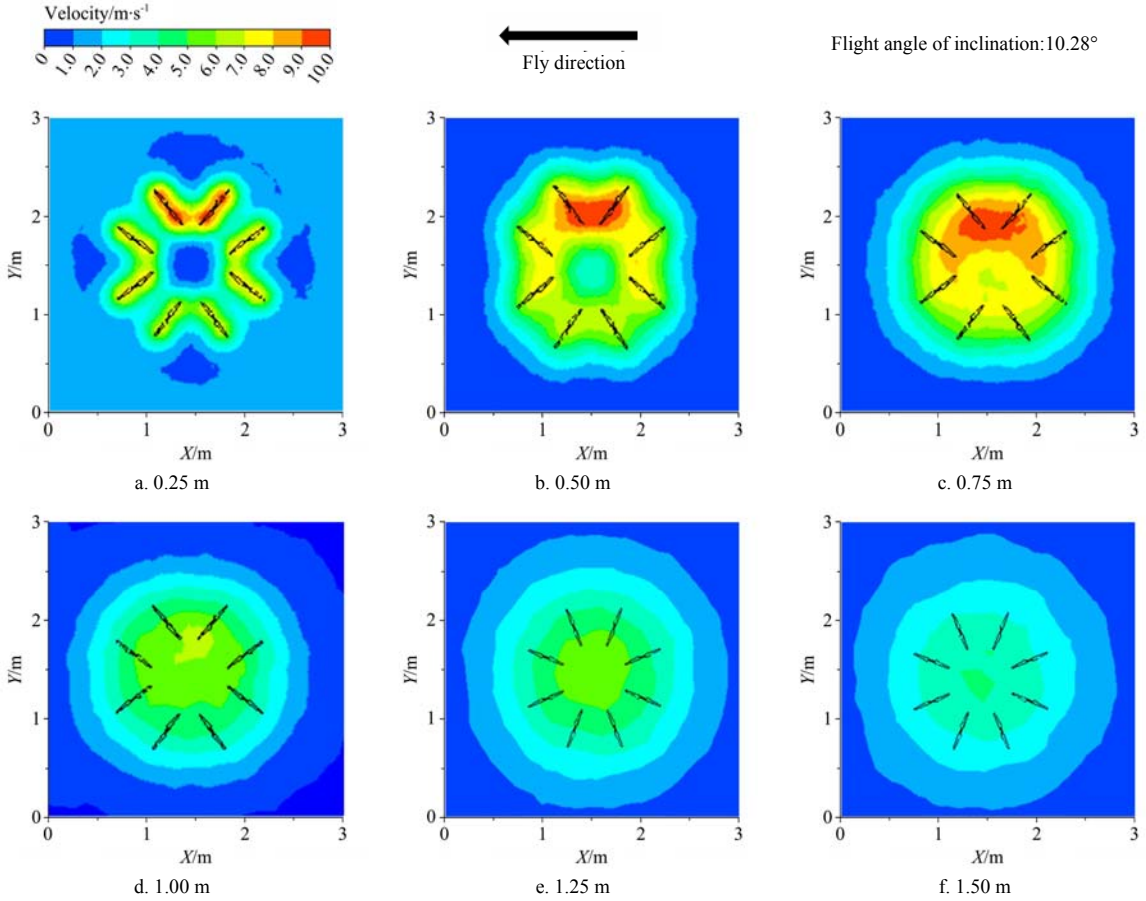


Figure 5 Downwash distribution map below the rotor

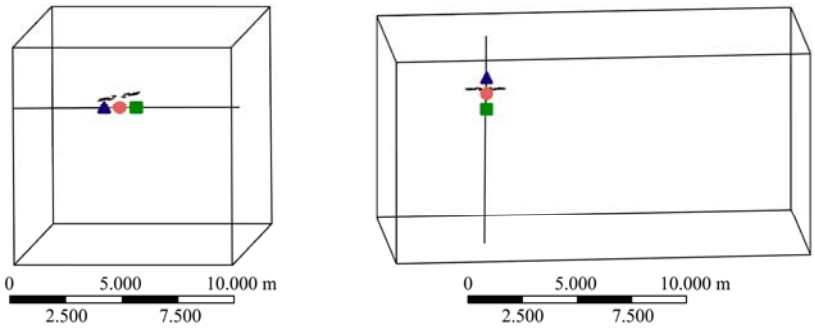


Note: In Figure 6a, triangle, round, and square blocks in horizontal line below rotors represent three points of "forward", "middle", and "behind". In Figure 6b: Triangle, round, square blocks in vertical line through rotors represent three points of upper, middle, lower.

Figure 6 Established lines in computational domain

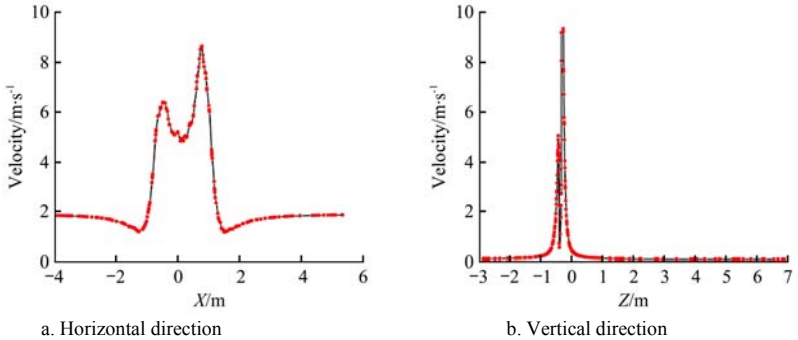


Figure 7 Downwash distribution below the rotor in different directions

### 4.2 Droplet Drift and Deposition

The drift and deposition of particle were described by particle trapped method and the droplet drift rate can be calculated by Equation (4).

$$D_d = N_d / N_t \times 100\% \quad (4)$$

where, $D_d$ means droplet drift rate, %; $N_d$ means the number of droplet drift; $N_t$ means the number of total droplets.

4.2.1 Droplet drift influenced by downwash

Flight angles of inclination (10.28°) and wind speed (3 m/s) were set to constant and the effects of downwash were explored. Two groups of simulation analysis were respectively set to open and close, the results are shown in Figure 8. The domain was divided into the target area and drift area by a vertical plane, the distance between the UAV center and this plane was 3 m, half of spray swath width.

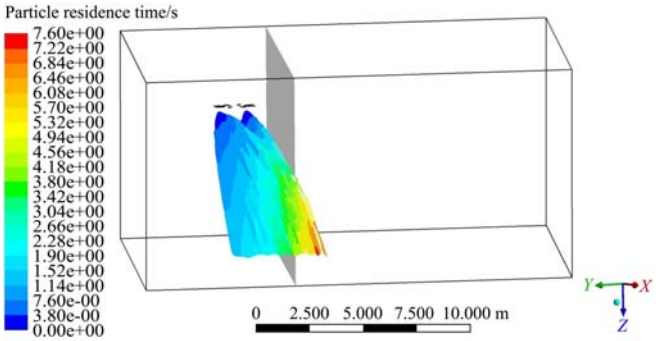


a. Close

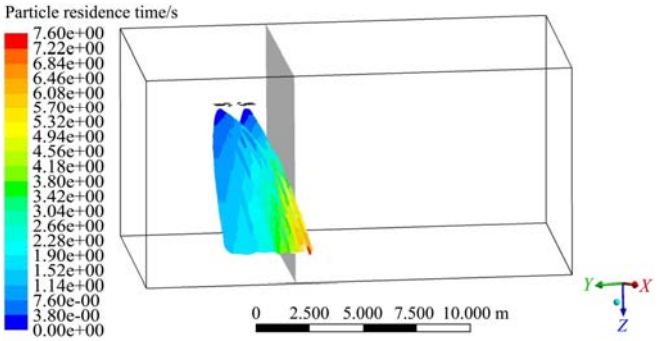


b. Open

Note: The wall parallel to velocity inlet of left plane represents the boundary between target area and off-target area according to spraying swath width.

Figure 8 Contract of droplet drift in different downwash

When downwash was open, the droplet drift rate was 23.5% and when downwash was close, the droplet drift rate was 31.5%. The depressant effects of downwash to droplet drift can be proved.

4.2.2 Droplet drift influenced by flight angle of inclination

Wind speed (3 m/s) and downwash (open) were set to constant and the effect of flight angle of inclination of 2.46°, 5.19°, and 10.28° were explored. The results are shown in Figure 9.

The droplet drift rate of the three groups were 5.2%, 12.9%, and 23.5%, so the droplet drift rate increase as the flight angle of inclination increases which indicates they are positively correlated.

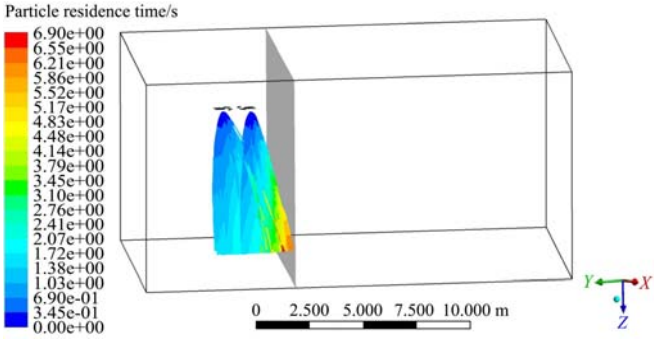


a. 2.46°

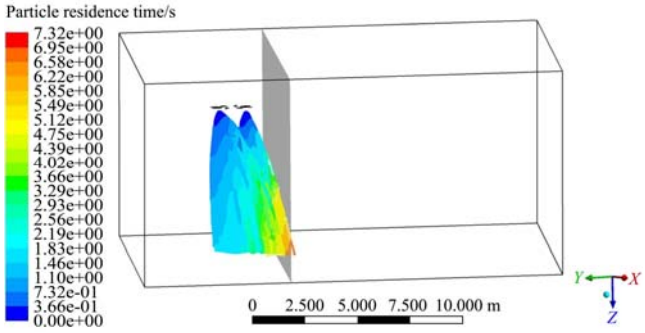


b. 5.19°

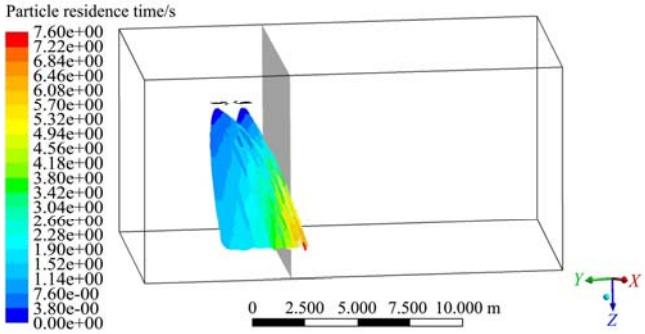


c. 10.28°

Figure 9 Contract of droplet drift in different flight angles of inclination

4.2.3 Droplet drift model

Totally nine simulation analyses were carried out to seek the law of droplet drift and drift rates in different conditions are shown in Table 7 and Figure 10.

**Table 7 Drift droplet number and drift rate (in bracket) in different variable combination**

| Wind speed /m·s$^{-1}$ | Flight angle/(°) | | |
|---|---|---|---|
| | 2.46 | 5.19 | 10.28 |
| 0 | 2 (0) | 234 (2.9%) | 318 (4%) |
| 1 | 92 (1.1%) | 773 (9.7%) | 1103 (13.8%) |
| 3 | 1048 (13.1%) | 2302 (28.8%) | 3108 (3.9%) |

Note: The percentage in bracket means drift rate calculated by drift droplet number and total droplet number.

The data was collected in flight angle was 2.46°,5.19°, and 10.28° separately and the wind speed were 0 m/s, 1 m/s, and 3 m/s.

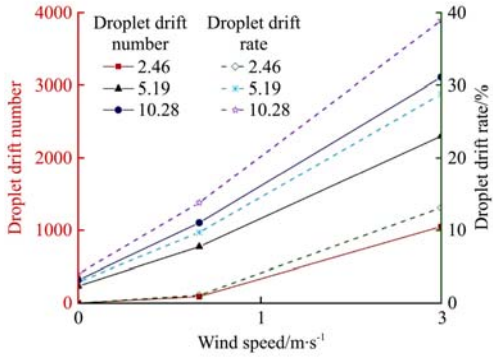


Figure 10 Droplet drift number and rate in different flight angles under different wind speeds

It can be seen that the number of droplet drifts is positively correlated with flight angle of inclination and wind speed. According to the figure above, the least square method was taken to fit a curve of droplet number drift. The variance and regression analysis of the influence of flight angle of inclination and wind speed on the number of droplet drifts is shown in Table 8.

**Table 8 Variance and regression analysis of the influence of three factors on droplet drift number**

| Factor | Regression coefficient | T-distribution value | Significance | 95% Confidence interval | | $R$ | $R^2$ |
|---|---|---|---|---|---|---|---|
| | | | | Lower limit | Upper limit | | |
| Wind speed | 8.367 | 5.918 | ** | 4.908 | 11.827 | | |
| Flight angle | 1.758 | 3.109 | * | 0.374 | 3.142 | 0.939 | 0.882 |
| Constant term | −8.942 | −2.135 | * | −19.192 | 1.308 | | |

Note: The significances are the results of significance analysis and the number of stars means the degree of influence by independent variables. The two stars (**) means the influence is very significant, one star (*) is significant, and no star is not significant.

According to the analysis results (Table 8), the influence of wind speed on droplet drift number is very significant and the influence of flight angle of inclination droplet drift number is significant, so a linear equation can be established. The regression coefficients of three variables in the regression equation of droplet drift number are 8.367, and 1.758, and the constant term (C) is −2.135. Therefore, the relationship model between droplet drift number $Y$ and wind speed $X_w$ (m/s), flight angle of inclination $X_a$ (°) is

$$Y = 8.367X_w + 1.758X_a - 8.942 \ (R^2 = 0.957) \quad (5)$$

### 4.3 Two methods for reducing droplet drift

As shown in Figure 11, droplet particles were deposited behind the rotor because of the flight angle of inclination, this part of drift particles get out of downwash's control. To avoid this impact to reduce the droplet drift, two methods were put forward and a full simulation was carried out to prove their rationality.

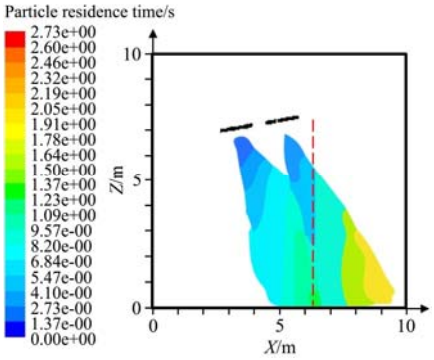


Note: Dotted line means the boundary line and right-side droplets get out of downwash's control.

Figure 11 Droplet drift influenced by flight angle of inclination

#### 4.3.1 Nozzle installation position

Droplet deposition can be moved forward by advancing nozzle position. Compared to the initial nozzle position, ten simulation groups (5 cm, 10 cm, 15 cm, 20 cm, 25 cm, 30 cm, 35 cm, 40 cm, 45 cm, and 50 cm) of different distances were carried out to figure out the best distance to advance. The results acquired are listed in Table 9 and the drift model fitted is shown in Figure 12.

**Table 9 Droplet drift number in different advanced distance**

| Advance distance/cm | Droplet drift number |
|---|---|
| 0 | 773 |
| 5 | 771 |
| 10 | 766 |
| 15 | 732 |
| 20 | 715 |
| 25 | 703 |
| 30 | 691 |
| 35 | 664 |
| 40 | 652 |
| 45 | 671 |
| 50 | 683 |

The nozzle advance distance($X$) model was

$$Y = 0.106X^2 - 8.676X + 844.6 \ (R^2 = 0.943) \quad (6)$$

According to the model fitted, the best nozzle advance distance was 40.9 cm. Compared to the initial droplet drift rate of 9.6%, the droplet drift rate decreased by 1.3 percentage points. A clear relationship between distance and droplet drift number can be seen in Figure 12, which shows suppression effect of droplet drift phenomenon by nozzle advance. Besides, proper distance selection should be taken into account because extra distance has an adverse effect. This method can be applied to plant protection UAV design process under the premise of ensuring overall rationality of structure. Whether it is necessary to move nozzle forward for a 1.3% drift decrease at the expense of symmetrical layout is another consideration.

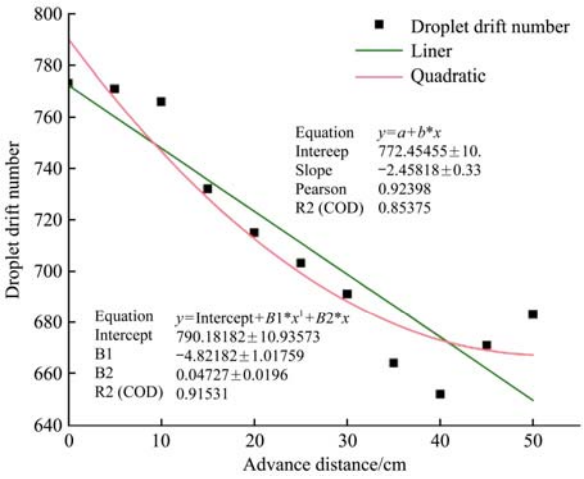


Figure 12 Fitted model of nozzle advance distance

#### 4.3.2 Nozzle body with inclination compensated

The use of nozzle body with inclination compensated can compensate the flight angle of inclination. Similar to nozzle advance, the droplet drift rate increases 3.5 percentage points from 9.6% to 6.1% after using nozzle body with inclination compensated. Explanation of mechanism analysis would be the flight angle of inclination compensation by using nozzle body with inclination compensated. Compared to the previous method, nozzle body with inclination compensated needs not to calculate the best distance. Although droplet drift rate can decrease by 3.5%, design difficulty of nozzle body exists.

## 5 Discussion

Spray performance will be a major consideration in the employment stage of plant protection UAV products. Full research containing droplet drift, deposition, and their factors were reported by the combination of experiment and simulation. First, an actual experiment was applied, and the information collected from these experiments provided valuable insight into the behavior of rotors and the change of flight angle applied from multirotor plant protection UAVs. General observations suggest that the rotor rotation speed difference and flight angle vary significantly

with different operation speeds. Additionally, rotors can be divided into three groups, forward, middle, and behind neglecting slight roll and pitch motion. Second, according to parameters from the experiment, a simulation based on CFD was applied concerning model building, parameters setting, case solution, and result analysis. Downwash flow analysis shows a slight difference in value between groups and a similar change tendency from rotor center to edge areas. At last, we put forward two methods to reduce droplet drift by avoiding getting rid of the downwash area. After calculating the best distance, artificially moving the nozzle forward to reduce drift is a feasible approach. In addition to nozzle advance, nozzle body with inclination compensated is also a method although this will bring some difficulty to design.

## 6 Conclusions

In this study, the CFD simulation method was used to acquire droplet deposition distribution and drift under the influence of different factors. DPM model was used to simulate droplet drift from a double XR8002 nozzle at various wind speeds (0, 1 m/s, 3 m/s), and operation speeds (1-3 m/s, 3-5 m/s, 5-7 m/s) according to the actual experiment. General analysis from the actual experiment suggests that the droplet drift was significantly influenced by the flight angle of inclination and wind speed. The information obtained from these simulations shows the characteristic of spray drift and downwash. Additionally, although two methods of reducing drift have been proved by simulation analysis, detailed actual experiment should be carried out to prove. Results made from these simulations have provided a tool that can be used to ensure future UAV chemical application can be designed to maximize efficacy, reduce waste, and minimize damage to organisms not being targeted.

## Acknowledgements

This work was partially financially supported by the National Key R&D Program of China (Grant No. 2016YFD0200701).

## [References]

[1] Zhang C, Kovacs J M. The application of small unmanned aerial systems for precision agriculture: A review. Precision Agriculture, 2012; 13: 693–712.

[2] Zhang N, Wang M, Wang N. Precision agriculture - A worldwide overview. Computers and Electronics in Agriculture, 2002; 36(2–3): 113–132.

[3] Kirk I W, Fritz B K, Hoffmann W C. Aerial methods for increasing spray deposits on wheat heads. 2004 ASAE Annual Meeting, 2004; Paper No. 041029. doi: 10.13031/2013.16132.

[4] Fritz B K. Role of atmospheric stability in drift and deposition of aerially applied sprays - Preliminary results. 2004 ASAE Annual Meeting, Paper No. 041031. doi: 10.13031/2013.16143.

[5] Bilanin A J, Teske M E, Barry J W, Ekblad R B. AGDISP: The aircraft spray dispersion model, code development and experimental validation. Transactions of the ASAE, 1989; 32(1): 327–334.

[6] Teske M E. An introduction to aerial spray modeling with FSCBG. Forest Service Cramer-Barry-Grim. Journal of the American Mosquito Control Association, 1996; 12: 353–358.

[7] Hewitt A J. Spray drift: Impact of requirements to protect the environment. Crop Protection, 2000; 19(8–10): 623–627.

[8] Hewitt A J, Johnson D R, Fish J D, Hermansky C G, Valcore D L. Development of the spray drift task force database for aerial applications. Environmental Toxicology and Chemistry, 2002; 21(3): 648–658.

[9] Teske M E, Bird S L, Esterly D M, Curbishley T B, Ray S L, Perry S G. AgDRIFT®: A model for estimating near-field spray drift from aerial applications. Environmental Toxicology and Chemistry, 2002; 21(3): 659–671.

[10] Teske M E, Thistle H W, Riley C M, Hewitt A J. Initial laboratory measurements of the evaporation rate of droplets inside a spray cloud. Transactions of the ASABE, 2016; 59(2): 487–493.

[11] Fesal S N M, Fawzi M, Omar Z. A numerical analysis of flat fan aerial crop spray. IOP Conference Series: Materials Science and Engineering, 2017; 243: 012044. doi: 10.1088/1757-899X/243/1/012044.

[12] Wilson C, Tisdell C. Why farmers continue to use pesticides despite environmental, health and sustainability costs. Ecological Economics, 2001; 39(3): 449–462.

[13] Xue X Y, Lan Y B, Sun Z, Chang C, Hoffmann W C. Develop an unmanned aerial vehicle based automatic aerial spraying system. Computers and Electronics in Agriculture, 2016; 128: 58–66.

[14] Jiao L Z, Dong D M, Feng H K, Zhao X D, Chen L P. Monitoring spray drift in aerial spray application based on infrared thermal imaging technology. Computers and Electronics in Agriculture, 2016; 121: 135–140.

[15] Li J Y, Shi Y Y, Lan Y B, Guo S. Vertical distribution and vortex structure of rotor wind field under the influence of rice canopy. Computers and Electronics in Agriculture, 2019; 159: 140–146.

[16] Guo S, Li J Y, Yao W X, Zhan Y L, Li Y F, Shi Y Y. Distribution characteristics on droplet deposition of wind field vortex formed by multi-rotor UAV. PLoS One, 2019; 14(7): e0220024. doi: 10.1371/journal.pone.0220024.

[17] Dorr G J, Forster W A, Mayo L C, McCue S W, Kempthorne D M, Hanan J, et al. Spray retention on whole plants: Modelling, simulations and experiments. Crop Protection, 2016; 88: 118–130.

[18] Ellis M C B, Miller P C H. The Silsoe spray drift model : A model of spray drift for the assessment of non-target exposures to pesticides. Biosystems Engineering, 2010; 107(3): 169–177.

[19] Wen S, Han J, Ning Z H, Lan Y B, Yin X C, Zhang J T, et al. Numerical analysis and validation of spray distributions disturbed by quad-rotor drone wake at different flight speeds. Computers and Electronics in Agriculture, 2019; 166: 105036. doi: 10.1016/j.compag.2019.105036.

[20] Ryan S D, Gerber A G, Holloway A G L. A time-dependent Eulerian model of droplet diffusion in turbulent flow. Computers and Fluids, 2016; 131: 1–15.

[21] Zhang B, Tang Q, Chen L P, Xu M. Numerical simulation of wake vortices of crop spraying aircraft close to the ground. Biosystems Engineering, 2016; 145: 52–64.

[22] Yang F B, Xue X Y, Cai C, Sun Z, Zhou Q Q. Numerical simulation and analysis on spray drift movement of multirotor plant protection unmanned aerial vehicle. Energies, 2019; 11(9): 2399. doi: 10.3390/en11092399.

[23] Omar Z, Qiang K Y, Mohd S, Rosly N. CFD simulation of aerial crop spraying, In: IOP Conference Series: Materials Science and Engineering, 2016; 160: 012028. doi: 10.1088/1757-899X/160/1/012028.

[24] Zhu H, Li H Z, Zhang C, Li J X, Zhang H H. Performance characterization of the UAV chemical application based on CFD simulation. Agronomy, 2019; 9(6): 308. doi: 10.3390/agronomy9060308.

[25] Li L, Qi H, Yin Z, Li D, Zhu Z, Tangwarodomnukun V, et al. Investigation on the multiphase sink vortex Ekman pumping effects by CFD-DEM coupling method. Powder Technology, 2019; 360: 462–480.

[26] Vahabzadeh M, Hossein M, Hong K, Xiong Q. CFD study of heat transfer and fl uid fl ow in a parabolic trough solar receiver with internal annular porous structure and synthetic oil-$Al_2O_3$ nanofluid. Renewable Energy, 2020; 145: 2598–2614.

[27] Li Y S, Tian Y, Tian J D, Zhou F. An efficient method for DPM code localization based on depthwise separable convolution. IEEE Access, 2019; 7: 42014–42023.

[28] Zhang L, Ji R Q, Fu Y F, Qi H, Kong F Z, Li H N. Investigation on particle motions and resultant impact erosion on quartz crystals by the micro-particle laden waterjet and airjet. Powder Technology, 2019; 360: 452–461.

[29] Duraisamy K, Iaccarino G, Xiao H. Turbulence modeling in the age of data. Annual Review of Fluid Mechanics, 2019; 51: 357–377.

[30] Mei J, Ren W, Ma G F. Distributed coordinated tracking with a dynamic leader for multiple Euler-Lagrange systems. IEEE Transactions on Automatic Control, 2011; 56: 1415–1421.